Development of a Bayesian network-based early warning system for storm-driven coastal erosion

J.L. Garzon [a,*], O. Ferreira [a], T.A. Plomaritis [b], A.C. Zózimo [c], C.J.E.M. Fortes [c], L.V. Pinheiro [c]

[a] *CIMA – Centre for Marine and Environmental Research, FCT, Universidade do Algarve, Campus de Gambelas, 8005-139 Faro, Portugal*
[b] *Faculty of Marine and Environmental Science, Department of Applied Physics, University of Cadiz, Campus Rio San Pedro (CASEM), Puerto Real 11510, Cadiz, Spain*
[c] *Hydraulics and Environment Department, National Laboratory for Civil Engineering, Av. do Brasil, 101, 1700-066 Lisboa, Portugal*

A B S T R A C T

Coastal hazards such as flooding and erosion can cause large economic and human losses. Under this threat, early warning systems can be very cost-effective solutions for disaster preparation. The goal of this study was to develop, test, and implement an operational coastal erosion early warning system supported by a particular method of machine learning. Thus, the system combines Bayesian Networks, and state-of-the-art numerical models, such as XBeach and SWAN, to predict storm erosion impacts in urbanized areas. This system was developed in two phases. In the development phase, all information required to apply the machine learning method was generated including the definition of hundreds of oceanic synthetic storms, modeling of the erosion caused by these storms, and characterization of the impact levels according to a newly defined eerosion iimpact index. This adimensional index relates the distance from the edge of the dune/beach scarp to buildings and the height of that scarp. Finally, a Bayesian Network that acted as a surrogate of the previously generated information was built. After the training of the network, the conditional probability tables were created. These tables constituted the ground knowledge to make the predictions in the second phase. This methodology was validated (1) by comparing 6-h predictions obtained with the Bayesian Network and with process-based models, the latest considered as the benchmark, and (2) by assessing the predictive skills of the Bayesian Network through the unbiased iterative *k*-fold cross-validation procedure. Regarding the first comparison, the analysis considered the entire duration of three large storms whose return periods were 10, 16, and 25 years, and it was observed that the Bayesian Network correctly predicted between 64% and 72% of the impacts during the course of the storms, depending on the area analyzed. Importantly, this method was also able to identify when the hazardous conditions disappeared after predicting potential consequences. Regarding the Regarding the second validation approach, second validation approach, the *k*-fold cross-validation procedure was applied to the peak of a set of varying storms and it demonstrated that the predictive skills were maximized (63%–72%) when including three nodes as input conditions of the Bayesian Network. In the operational phase, the system was integrated into the architecture of a forecast and early warning system that predicts emergencies in coastal and port zones in Portugal, and the alerts are issued to authorities every day. This study demonstrated that the two-phase approach developed here can provide fast and high-accuracy predictions of erosion impacts. Also, this methodology can be easily implemented on other sandy beaches constituting a powerful tool for disaster management.

1. Introduction

Natural hazards are causing gigantic economic losses and they are showing an increasing tendency in damages and socioeconomic impacts (NOAA National Centers for Environmental Information, 2022). Moreover, with climate change, these negative impacts will be highly exacerbated (IPCC, 2012). These unfavorable perspectives represent a big challenge for disaster response managers but also an opportunity to embrace more robust and efficient management strategies. This has instigated the management and scientific communities to pay special attention to new approaches such as machine learning (ML) techniques. ML is a particular method of Artificial intelligence that consists of a set of computer algorithms, methods and tools that aim to accomplish given tasks and use data to optimize their performance. Currently, ML is being

applied to improve early warning and alert systems, generate hazard and susceptibility maps through machine learning-based detection and forecast natural hazards, particularly floods, earthquakes, and landslides (Kuglitsch et al., 2022; Sun et al., 2020). Also, the expansion of quality data including Earth observational data (social media-driven, telecommunication data, and remote sensing), and simulation data (computational models) represents a crucial aspect for the strengthening of ML to estimate disaster-induced impacts (Kuglitsch et al., 2022; Sun et al., 2020).

Coastal scientists are part of this growing machine learning community and they are applying this technique to support morphodynamic studies and sediment transport management. Goldstein et al. (2019) reviewed more than 60 publications that investigate coastal sediment transport, coastal morphology, and coastal morphodynamics through the application of ML techniques. The focus of these studies was the supervised learning method that allows for predicting continuous dependent variables. Supervised learning connects input and output data (e.g., wave forcing and shoreline change) aiming at obtaining a model which predicts a dependent variable based on a set of input variables. Therefore, such a model can imitate physical process interactions that are either poorly understood or too complex to be determined with deterministic models (Goldstein et al., 2019).

A variety of coastal morphology and morphodynamic models have been proposed by using machine learning techniques or combining morphodynamic models with machine learning (hybrid models). The most common machine learning techniques present in this field are (1) Artificial Neural Networks – ANN, e.g., Athanasiou et al. (2022), López et al. (2017) and Pape et al. (2010); (2) Genetic Algorithms – GA and Genetic Programming – GP, e.g., Goldstein and Moore (2016) and Grimes et al. (2015); (3) Multivariate Linear regression, e.g. Bruno et al. (2018), Charbonneau et al. (2017) and Garzon et al. (2022a); and (4) Bayesian Networks – BNs, e.g., Gutierrez et al. (2011), Plant and Stockdon (2012) and Poelhekke et al. (2016). The reader is referred to Goldstein et al. (2019) for a comprehensive review of these models.

Among these techniques, BNs are highly suitable for coastal morphodynamic predictions (Plant and Stockdon, 2012) while being more interpretable than other ML methods (Mihaljević et al., 2021). BNs are based on a joint probability distribution over the random variables of a domain, and hence, they can predict the values of a continuous response variable (Mihaljević et al., 2021), namely coastal vulnerability, barrier island morphodynamics, shoreline change, beach erosion, etc., given the values of some explanatory variables (e.g., oceanic conditions, foredune and beach morphology, sea-level-rise rate, etc.). This relation between variables can be easily visualized through the graphical representation of the network structure.

In the BNs, the variables are represented as the nodes of a directed acyclic graph and its arcs are interpreted as potential dependences between variables. This structure is normally given by a domain expert (Mihaljević et al., 2021). Since nodes are modeled utilizing probability distributions, risk and uncertainty can be estimated more accurately than in models where only mean values are taken into account, and this makes BNs very feasible for modeling environmental systems (Aguilera et al., 2011). The conditional probability tables (CPT) of the BNs can be learned automatically from modeled or observed data. Once the structure and CPT of the BN are specified, they constitute a powerful tool for inference (Mihaljević et al., 2021). If the structure is relatively simple, BNs can predict changes in distributions instantly and can be interpreted intuitively (Aguilera et al., 2011). For this reason, BNs have been used for coastal risk analysis and early warning systems (Banan-Dallalian et al., 2023; Callens et al., 2022; Dongeren et al., 2018; Garzon et al., 2023a; Jäger et al., 2018; Pearson et al., 2017; Plant and Stockdon, 2012; Plomaritis et al., 2018; Sanuy et al., 2020; Sanuy and Jiménez, 2021; van Verseveld et al., 2015) where their learning data can be obtained from observations or numerical simulations. In this latter approach, the BN act as a surrogate of the numerical models.

The goal of this study was to develop, test, and implement an operational early warning system (EWS) for coastal erosion in sandy beaches supported by machine learning techniques. The philosophy underpinning the conceptualization of this coastal erosion EWS was to minimize the time employed to create operational warnings while providing the end-users robust scientific-based information obtained from open sources and state-of-the-art numerical models and data-driven techniques. To achieve that, the systems were designed to function in two different phases, the development phase and the operational phase (Fig. 1). In the first phase (the development phase), the storm events were schematized, all the numerical model runs were performed, the associated impact levels were computed, the Bayesian Network was designed and the CPT that link storm characteristics and impacts were generated (Fig. 1). The development of this phase drew inspiration from the proof of concept study Poelhekke et al. (2016) with important improvements such as enhancing the model approach to downscale hydraulic conditions from deeper waters, extensive model calibration and validation, accounting for hourly predictions instead of only peak storm predictions, more sophisticated hazard assessment and larger dataset for training. In the second phase (operational), firstly, regional oceanic predictions are extracted daily. Then, this information is introduced as the explanatory variables into the BN, which acts as a surrogate of the previously generated information, and qasi-instantaneously outputs the impact levels, which are disseminated among the coastal authorities (Fig. 1). Further details of every element of both phases are provided in Section 3 and Section 4. Praia de Faro, on the southern coast of Portugal, was selected as a validation case. After assessing the suitability of this approach, the EWS was implemented in HIDRALERTA (Fortes et al., 2014, 2020), a forecast and early warning system that predicts emergency situations in coastal and port zones in Portugal.

2. Study area

Praia de Faro is an open sandy beach located in a narrow peninsula (Ancão) in the westernmost part of the Ria Formosa barrier island system, which is located on the southwestern coast of the Iberian Peninsula (Fig. 2A and B). Astronomical tides are semi-diurnal, with an average range of 1.3 m for neap tides and 2.8 m for spring tides. Also, the observed storm surge levels are relatively low (<0.6 m) (Ferreira et al., 2019) and the corresponding value for a return period of 50 years is around 0.7 m (Rodrigues et al., 2012). Therefore, the tides primarily dominate the variability of the total water level. Regarding the wave climate at Praia de Faro, it is highly influenced by the triangular-shaped system of Ria Formosa whose western and eastern flanks present orientations of 128°N and 60°N, respectively (Fig. 2A and B). Thus, this geometry makes the study site (in the western flank) more exposed to the dominant and more energetic wave conditions (W–SW), while it is fairly protected against the less energetic E–SE waves. Praia de Faro exhibits a steep and narrow beach face with a single or double berm. Sediments are medium to very coarse sand with d_{50} (median diameter particle size) of about 0.5 mm (Vousdoukas et al., 2012). Previous authors have classified the site based on the conceptual model of Masselink and Short (1993) as reflective to intermediate (e.g. Almeida, 2007; Ferreira et al., 1997; Haerens, 2009). The average beach face slope observed by various authors varies between 0.11 (Ferreira et al., 1998) and 0.14 (Ciavola et al., 1997).

The EWS was designed for the stretch of the Ancão peninsula where urban development is intense (Fig. 2). The oceanfront is protected by rocks (mostly buried by sand) or walls and naturally by a beach-dune system. The dune elevation varies alongshore with higher elevation in the western sector of the study area. While some edifications were built close to the scarp edge in this sector, the natural system has not been fully destroyed (Fig. 2C). Conversely, in the parking sector, the dune was replaced by houses and infrastructures (Fig. 2D). In the central sector, a foredune is minimally present in some portions while in others, it was destroyed (Fig. 2E). In the eastern sector, the anthropogenic impact on the dune crest is less important and the dune is better preserved than in
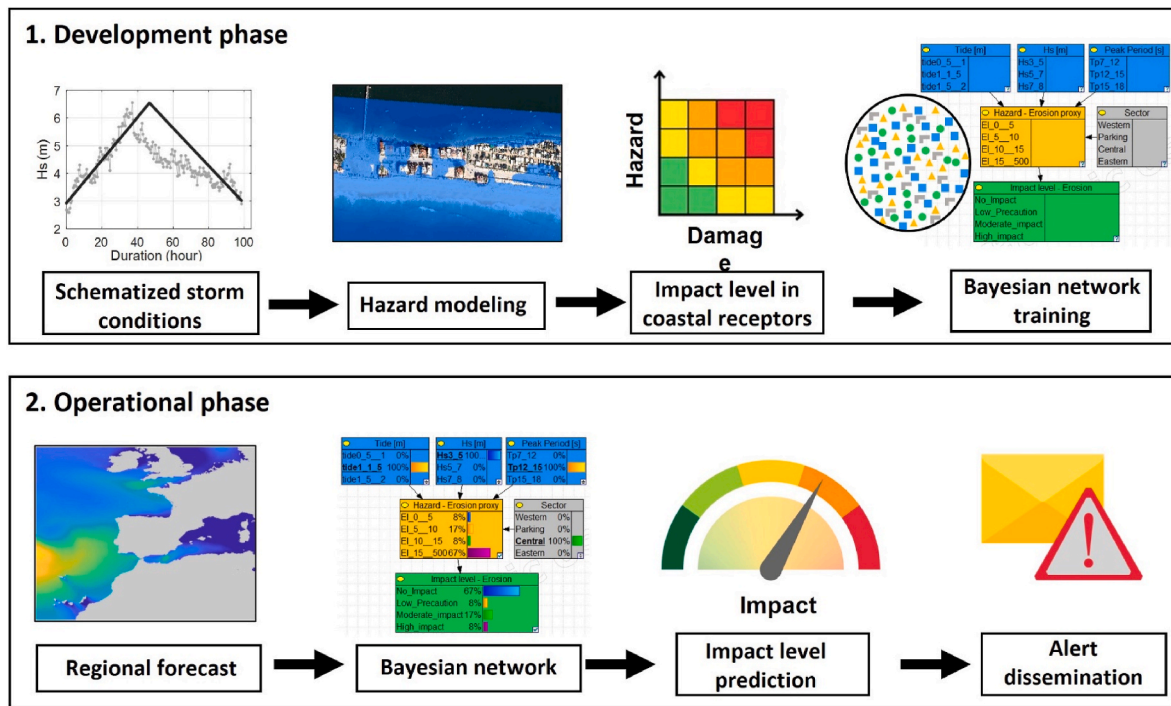
Fig. 1. Overview of the EWS for coastal zones with the two functional phases.

the two previous sectors (Fig. 2F). This division depended mainly on the exposure of the receptors of each sector.

3. Development phase

3.1. Storm schematization and boundary conditions

One of the most important requirements of the BNs is the availability of quality data to generate CPT. Here, this information was obtained by running calibrated and validated process-based models for a set of boundary conditions (BC). Since the BNs need to be trained over the whole range of possible events, it was not possible to obtain this information from observations and instead, the copula methodology was used to create this set of synthetic events (Fig. 1). The methodology to create the BC involved the following steps:

(1) Using a multivariate statistical methodology presented in Poelhekke et al. (2016), 300 new synthetic storms represented by Hs, Tp, surge and duration were generated (Fig. 3). This approach applied the copula technique to account for the natural variability of the variables. The goodness of the copula behavior was carefully evaluated by Poelhekke et al. (2016) for this site, revealing a good fit (see Poelhekke et al. (2016) for a detailed explanation).

(2) Obtaining linear adjustments derived from a 20-year dataset of measurements at the Faro buoy and Huelva tidal gauge (representative of the study site) that explained Tp, storm surge and storm duration as a function of Hs, along with the 95% confidence bounds (Fig. 3). This linear dependence (and statistical significance), previously noticed also by Poelhekke et al. (2016), was only determined for W-SW wave directions since the E-SE events cannot create hazardous conditions in the urbanized area.

(3) Adjusting the copula-generated data. Most of the copula-generated variables that represented the storms were within the 95% observations-derived confidence boundaries (green crosses in Fig. 3). Yet, a few cases lay outside of these boundaries, which indicated that their probability of occurrence was very low when

compared to the observed data. This was also noticed by Poelhekke et al. (2016) that argued that this was due to the existence of unknown asymptotes associated with unknown physical limits. Therefore, these cases were adjusted to lay on the 95% confidence bounds obtained in step (2) (grey circles in Fig. 3). This procedure was considered appropriate for the purpose of adjusting the data from outside the bounds and only affected a reduced number of cases (4.3% for the surge variable, mostly when Hs < 4.5 m, 2.6% for the duration variable and 0.7% for the Tp variable). It is important to note that the linear adjustments computed in step (2) were only used to adjust the copula-generated data.

(4) Establishing the oceanic variables used as explanatory variables in the BN and their discretization based on the findings of previous studies (Plomaritis et al., 2018; Poelhekke et al., 2016). Therefore, three variables were considered: Hs, Tp, and tide level. Regarding their discretization, three bins were used (0.5–1.0 m, 1.0–1.5 m, and 1.5–2.0 m) for the tide conditions, five 1.5 s-size and one 3.0 s-size bins were considered for Tp, and for Hs the number of bins considered was ten and the bin size was constant, 0.5 m (Fig. 4).

(5) Selecting the storms to be part of the training information. The density of events per Hs-Tp pair varied as the copula methodology was able to characterize the natural likelihood of occurrence of these variables (Fig. 4). To limit the number of storms to be simulated, a maximum of four storms per bin was considered (blue crosses in Fig. 4). This number was established based on the bin size of the Hs and Tp variables and it was in agreement with previous studies such as Poelhekke et al. (2016). The selection was based on the "k points the farthest apart" criteria, which accounted for the normalized distance of four variables such as Hs, Tp, surge and duration. Then, the storms whose variables had the longest normalized distance between themselves were selected to account for the highest storm variability.

(6) Complementing the copula-generated data. The Hs-Tp pairs with no copula data were separated into low occurrence but naturally feasible (black circles in Fig. 4) and non-naturally feasible. As BNs
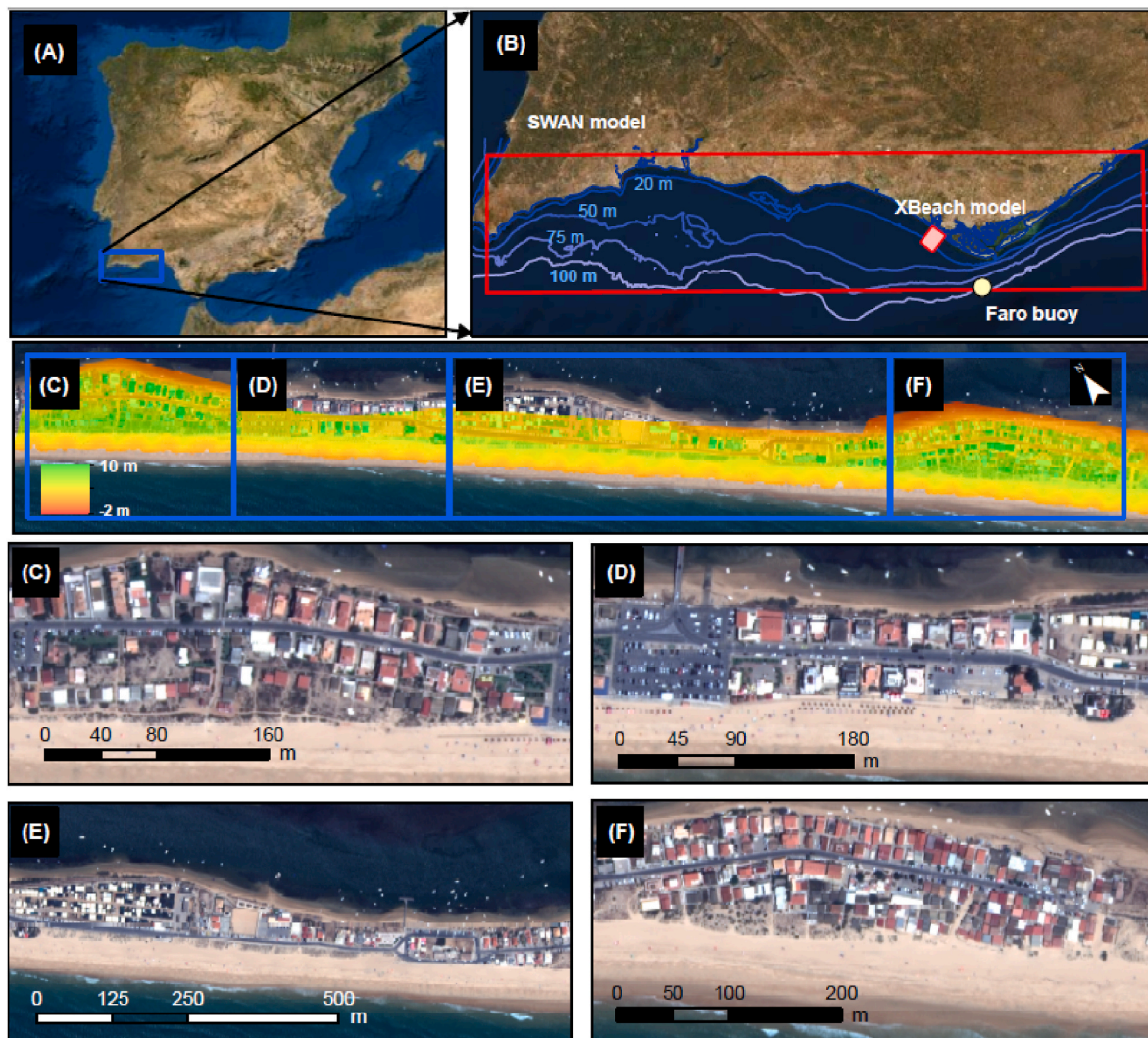
Fig. 2. (A) The Iberian Peninsula with the blue box highlighting the southern region of mainland Portugal. (B) The numerical model domains and the Faro buoy location. Source: Esri, DigitalGlobe, GeoEye, Earthstar Geographics, CNES/Airbus DS, USDA, USGS, AeroGRID, IGN, and the GIS User Community. Terrain elevation and the aerial view of the stretch of Praia de Faro where the EWS was implemented and the four sectors investigated: (C) Western, (D) Parking, (E) Central and (F) Eastern. Imagery source: Garzon et al. (2022a).

cannot extrapolate beyond the training data, it is very important to consider the possible storm conditions. Thus, for the first group (black circles in Fig. 4), mainly located above the grey squares in Fig. 4, new storms were generated by using the Hs and Tp values centered in their pair (Fig. 4, bins with one centered cross and one circle). In the second group, the wave steepness would exceed the values found in the study area according to the analysis conducted by Mendes and Oliveira (2021), and therefore no BC data were generated for those Hs-Tp pairs (Fig. 4, bins without crosses, circles or squares). Thus, 138 storms, defined by Hs, Tp, surge and duration, were selected.

(7) Defining the temporal evolution of the storm parameters. After obtaining the parameters that characterized a synthetic storm, its evolution was schematized following the symmetrical triangular shape simplification approach, which assumed a linear increase of the Hs and surge, until reaching the peak of the storm at half of the storm duration with the subsequent symmetric decrease of the Hs and surge level. The peak period during the storm followed also a triangular symmetric evolution and the ascendent and descendent slopes were calculated assuming a constant wave steepness value. This value was computed for the Hs and Tp provided by the copula methodology (Plomaritis et al., 2018).

This approach was already tested and validated for a large storm in Praia de Faro (Ferreira et al., 2019; Plomaritis et al., 2019b) revealing an overall good performance. Also, in deeper investigations conducted by Garzon et al., 2023b, it was found that the differences in berm and dune retreat between the synthetic and real storm accounted for up to 17% and 26% respectively, which might be considered acceptable. To compute the water levels, three tide elevation timeseries at this site that represented from neap to spring tides and whose maximum elevations were 0.8 m, 1.20 m and 1.56 m above mean sea level (Plomaritis et al., 2018) were added to the surge evolution. Hence, the water level evolution of each storm simulated with XBeach included both tide and surge. The timing between the maximum Hs and the highest tidal level was set to vary randomly for a period of ±2 days and the temporal resolution of these synthetic storms was 1 hour. Therefore, in total 414 synthetic storms (138 storms times three tide conditions) were generated to create the BC and each set of 138 storms was used to populate each bin of the tide variable in the training process.

It is important to highlight that for a more efficient implementation of the methodology, the duration and surge were not included as inputs
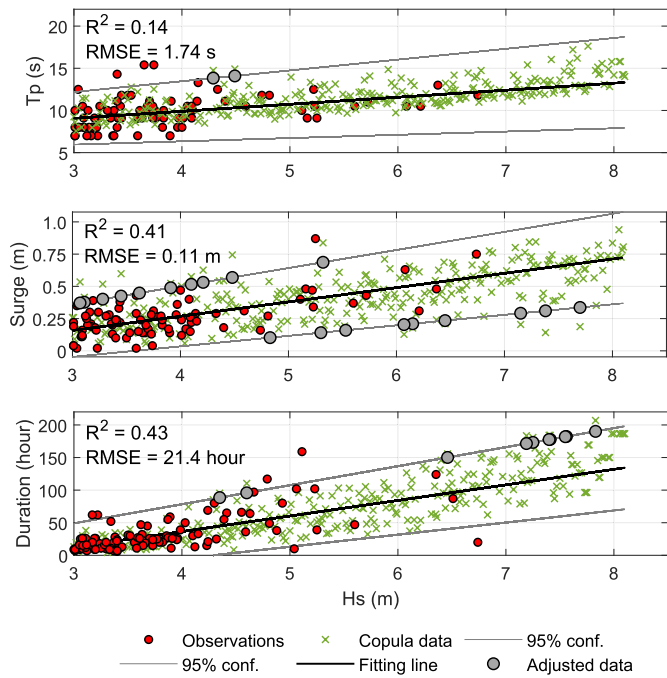
Fig. 3. Observed Hs against Tp, surge and duration (red dots) with the fitting line that explains the observations and the 95% confidence boundaries. The green crosses display all the copula generate data and the grey circles show the copula adjusted data (within the 95% confidence boundaries).
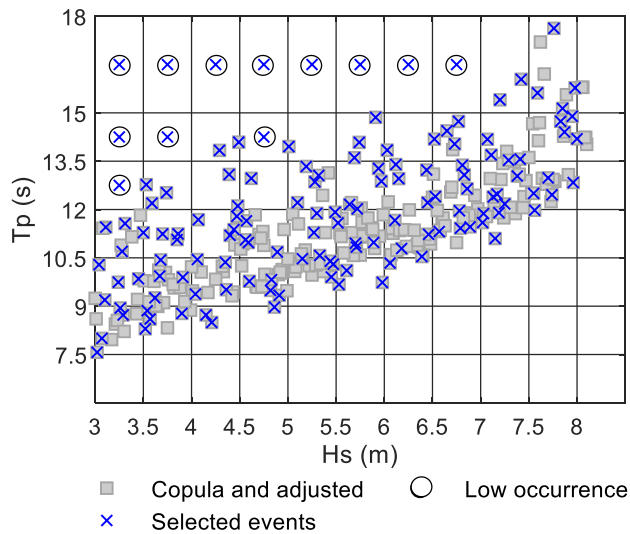

Fig. 4. All copula and adjusted storms (grey squares) characterized by Hs against Tp, the low occurrence probability events (black circles) and the selected storms to train the BN (blue crosses).

of the BN, but were internally accounted for in the simulations, with the natural variability of these variables being introduced by the copula method, as displayed in Fig. 3. By disregarding duration and surge as explanatory variables of the BN, the training dataset was reduced and therefore the total computational time. Moreover, when the values of the oceanic explanatory variables were below the lowest corresponding bin of the BN, the impact was assumed to be null (no impact).

3.2. Hazard numerical modeling

All developed synthetic storms were implemented into a numerical

framework formed by SWAN (Booij et al., 1999) + XBeach (Roelvink et al., 2009) models that simulated coastal erosion at the site (Fig. 1). The model results and the derived impacts were key for creating the training for the Bayesian Network, a fundamental aspect for the development of a reliable prediction when using machine learning. The SWAN (v41.31) model grid covered the entire southern Portuguese coast (Fig. 2B) since the domain was laterally expanded to cover large adjacent areas to avoid lateral boundary effects in the study area for the modeled events (W–SW directions). The model was forced with a JONSWAP wave spectra built from the wave parameters and gamma of 3.3 at the southern oceanic boundary located at 36.905°N and extended between 8.95°W and 7.50°W, where the water depth ranged between 70 m and 700 m with an average depth of 200 m (Fig. 2B). Water level variations and wind velocity were not considered in the SWAN simulations. The wave spectral resolution in space was 5° and the range of frequencies was divided into 34 parts, ranging from 0.0345 s^{-1} to 1 s^{-1}. The structured grid resolution was 350 m and 600 m in the cross-shore and alongshore directions, respectively. This model was used to propagate and downscale the wave conditions from the Faro buoy (~100 m depth) to 25 m depth, where the XBeach offshore boundary was located (Fig. 2B). A JONSWAP wave spectra built from the wave parameters modeled by SWAN and gamma of 3.3 were used for the offshore conditions of the XBeach simulations.

Then, XBeach version X 1.23.5526 was used to propagate the wave conditions to the shore and compute coastal erosion. To simulate this hazard, the surfbeat mode was considered. It solved morphodynamic processes, including bedload and suspended sediment transport, dune face avalanching, bed update and breaching. The Praia de Faro grid had an extension of 3 000 m longshore and 3 900 m cross-shore. The numerical grid was optimized by creating variable longshore and cross-shore grid cell spacing. The minimum cross-shore and alongshore resolution in the sub-aerial beach were 2 m and 10 m, respectively. Time series of water levels were imposed in the offshore boundary of the model and cyclic conditions were imposed in the lateral boundaries with the longshore gradient set to zero, i.e., there is locally no change in surface elevation and velocity (Neumann boundary condition). Roads, parking lots, infrastructures and building locations were identified, superimposed into the grid cells and set as a non-erodible layer (Fig. 5). This model was already calibrated and validated by Garzon et al. (2022b) against cross-shore profiles for 16-year and 5-year return period storms with Brier Skill Scores higher than 0.80, which indicated excellent performance according to the van Rijn et al. (2003) classification. An example of the erosion simulated by the numerical framework for one of the synthetic storms is illustrated in Fig. 5, where the four sectors are highlighted. The large alongshore variability is associated with the existence of beach cusps on the pre-storm morphology.

3.3. Storm impact assessment

To establish the potential danger driven by the collapse of buildings and infrastructures due to sand removal and destabilization of the foundation, four levels of impact have been established (Table 1). This classification displayed the traditional color code used in risk assessment studies, where green means safe, yellow represents precaution, orange indicates potential damage and red illustrates damage. This impact category was defined by using the newly proposed erosion impact (EI) index presented in Eq. (1). The EI index relates the horizontal distance (D) measured from the most seaside non-eroded point of the emerged profile (edge) to the target, namely buildings or other constructions (Fig. 6), and the height (h) of the dune or beach scarp (Fig. 6) following the expression:

$$\text{EI index} = \frac{D}{h} \tag{1}$$

The EI index assumed the formation of a vertical scarp, where h was computed as the difference in elevations between the edge and the
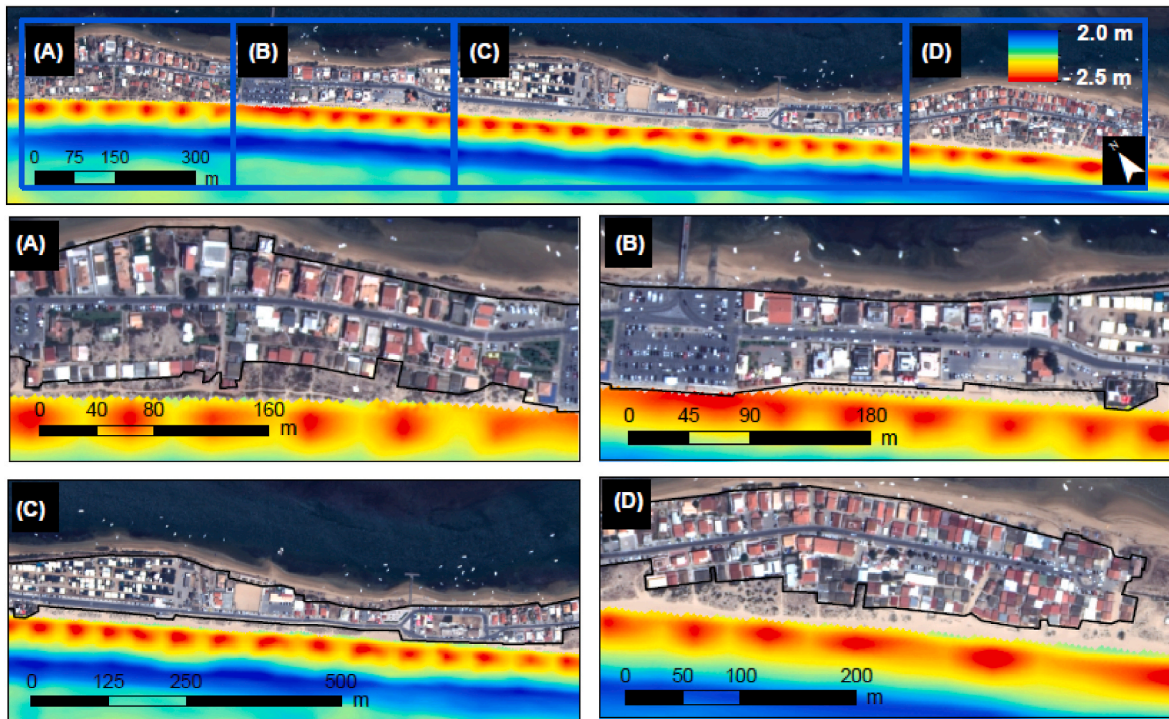
Fig. 5. Example of an XBeach model run. Warm colors represent erosion and cold color deposition. The black line displays the boundary of the non-erodible layer.

Table 1
Impact level definition and the associated thresholds.

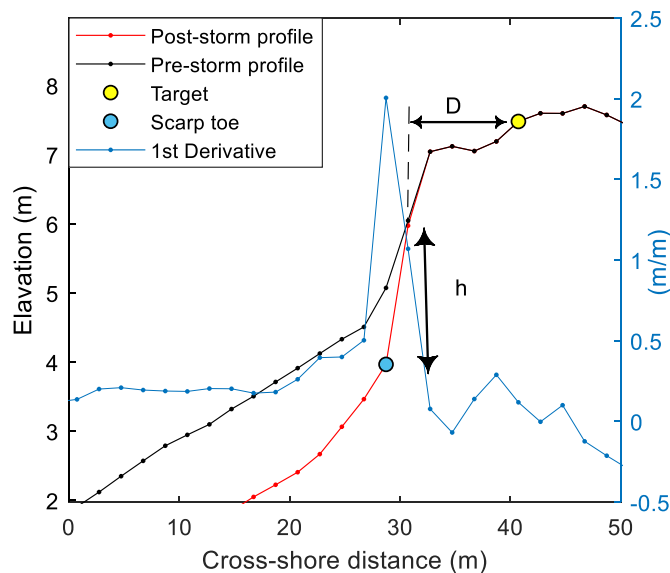| Impact Level	EI index
No Impact (Safe)	≥ 7.5
Low Impact (Precaution)	≥ 5.0 and <7.5
Moderate Impact (Potential damage)	≥ 2.5 and <5.0
High Impact (Damage)	<2.5

Fig. 6. Representation of the variables (D and h) involved in the calculation of the EI index.

elevation of the toe of the scarp (post-storm), as illustrated in Fig. 6. Following previous studies (Brodie and Spore, 2015), the toe of the scarp after the storm was defined as the location of maximum positive

curvature of the emerged eroded profile. Identifying the location of the dune toe can be very challenging and some authors have recognized limitations in the methods to automatically determine the coastal dune seaward boundary (Smith et al., 2020). However, without any additional information such as vegetation line or aerial or oblique images, the point of maximum curvature between the shoreline and dune crest can be a good indicator of the dune toe (Smith et al., 2020). Therefore, this approach is suitable and consistent as it easily allows for repeatability, without incorporating any human bias and intervention (vital in an operational system). Unlike previous studies (Sanuy and Jiménez, 2021), the proposed index assumed the hypothesis that both variables (a combination of D and h) can affect the structural stability of constructions. For example, for a D equal to 4 m, h values of 0.3 m and 1 m would result in no impact and moderate impact, respectively. For enhancing security, a conservative minimal h was set to 0.1 m to avoid cases where low values of h can increase the value of the EI index, and thus lead to an exaggerated reduction of the impact level prediction. Within each sector of the study area, the EI index was calculated at several cross-shore locations where the targets were highly exposed. Then, the lowest EI index was selected to characterize the impact along the entire sector.

The thresholds depicted in Table 1 were used to transform the hazards into impacts and were established based on the authors' judgment and after analyzing historical events and their impacts and consequences at Praia de Faro (Almeida et al., 2012; Ferreira et al., 2019; Garzon et al., 2022b). After the BC were generated, the 414 model runs were executed, the EI index for each sector was computed and the associated impacts were established based on the thresholds presented in Table 1, all the necessary information to develop the CPT of the BN was gathered. This information constituted the ground information of the BN-based EWS.

3.4. Bayesian network structure

The construction of the Bayesian Network required the definition of the input variables (nodes) and the dependencies between the variables (arcs). The direction of an arc, from so-called parent to child variables, represented the direction of influence. The BN design included four categories of variables: boundary conditions, receptor sector, hazards

and impacts. All BC and receptor sectors were mutually independent, while hazards and impacts were conditioned by their parents. This structure was based on the same principles as other BNs developed in previous studies at Praia de Faro (Poelhekke et al., 2016). The BC (blue boxes in Fig. 7) were represented as storm scenarios derived from a multivariate statistical analysis and divided into bins, as presented in section 3.1. The receptor sector (Fig. 2C–F and grey box in Fig. 7) was defined as a node that represented the location within the implementation area (Fig. 2). The EI index (hazards) corresponds to the yellow box in Fig. 7, whose bin sizes were defined based on the thresholds shown in Table 1. Finally, the impact level (green box in Fig. 7) indicates the impact level for specific BC and each sector. Therefore, the parent nodes such as tide level, Hs, Tp and sector, conditioned the EI index node, which itself conditioned the child node impact level. Then, the information generated in the previous sections (BC, sectors and impact levels) was used to train the BN and compute the CPT derived from joint probability distributions (Fig. 1) following the method described in Jäger et al. (2018). These CPT were written in text files. The training of the BN and computation of the CPT based on simulated impacts was the basis of the surrogate method that supported the EWS. Thus, for each set of initial oceanic conditions (i.e. waves and tide level) the final result (impact level) was provided by the BN, including the probabilities of

occurrence as illustrated for a particular example in Fig. 7. The visualization of the BN structure and the probabilities can be made through the graphical interface of the software Genie, which is freely available for academic research from BayesFusion, LLC (https://www.bayesfusion.com/).

3.5. Performance assessment of the surrogate method

The methodology behind the surrogate method, from the boundary condition generation up to the design, construction and training of the BN was validated by using two approaches based on: (1) a comparison of hourly BN and numerical model results for three large storms and (2) cross-validation for the peak of the storm.

3.5.1. Hourly comparison

Storm Emma with a 16-year return period event (Ferreira et al., 2019) and the 10-year and 25-year return period synthetic storm events were used to validate the proposed methodology. These two synthetic storms were created by considering the relationship between Hs and the rest of the variables defining a storm namely Tp, surge and duration (Garzon et al., 2023b). The Hs for each return period was obtained from previous studies such as Pires (1998). These three storms were
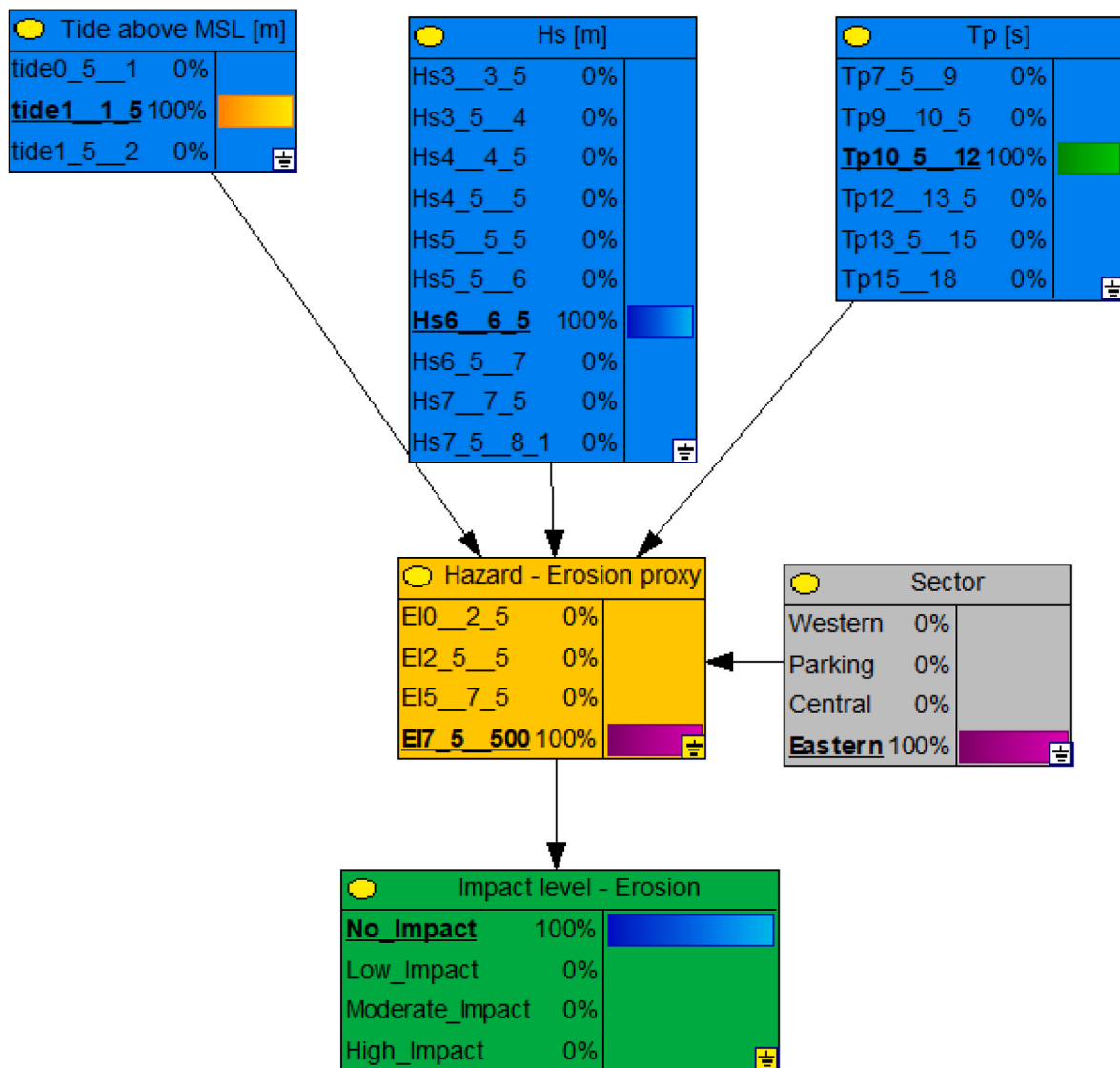

Fig. 7. Bayesian network structure including the boundary conditions (blue), sectors (grey), the hazard characterized as EI index (yellow) and the impact level (green). The selection of the BC corresponds to the peak of the storm Emma.

implemented in the process-based numerical model framework presented in Section 3.2, the EI index was computed and the associated impact levels were predicted every hour (hereafter referred to the non-surrogate method). Importantly, in the numerical simulations, if the EI index did not change over two or more consecutive hours, the considered impact was null except for the first hour which was calculated according to Table 1. Also, when the EI index reached a value of 0, high impacts were still predicted for the following hours if the scarp toe modified its elevation. This was necessary because infrastructures and houses were modeled as a non-erodible layer, and thus, the erosion cannot increase further beyond. This was especially relevant for the parking sector. This validation approach also allowed us to validate the timing of the impacts.

For validation, those impacts predicted by the non-surrogate method were compared against the impacts predicted by the BN (hereafter referred to the surrogate method). To this end, the same hourly storm conditions (tide level and wave parameters) were used as BC (explanatory variables) to predict the impacts. In the surrogate method, each hourly condition was considered as an independent storm. For example, at a given time during the course of the storm, the conditions could be $Hs = 4.1$ m, $Tp = 10$ s, and the tide level $= 0.9$ m. Thus, these values would be used to condition the BN and obtain a prediction. It means that this prediction was based on the training information from a set of 4 storms simulated with neap tides and whose max Hs varied from 4 m to 4.5 m, max Tp varied between 9 s and 10.5 s and each storm had a specific duration and surge given by the copula. Also, these simulations were initialized with a pre-storm profile.

It is important to mention that while the numerical framework provided deterministic results, the results of the BN were stochastic, i.e., in terms of probability distributions. However, for operational purposes, the impact level predicted by the BN was defined as the maximum level with a percentage of probability higher than 0%, if the addition of the remaining probabilities is lower than 66%. In the case that this condition was not satisfied, the impact level dropped one level. For instance, if the probability of a high impact was 50% and the probability of a low impact was 50%, then the released warning would be a high impact.

Nevertheless, if the probability of a low impact was 75% and the probability of a high impact was 25%, then the released warning would be a moderate impact. After testing several alternatives (not shown here), it was concluded that these criteria and conditions yielded the most accurate results when compared with the non-surrogate method for the three storms analyzed. Moreover, in order to simplify the warnings and facilitate the implementation of risk-reduction measurements, the BN predictions were integrated by selecting the highest impact level for a period of 6 hours centered on the peak of the tide level (i.e., 2 hours before, 1 hour representing the high tide and 3 h later).

The 6-hour integrated impact levels (the highest level in the grey areas in Fig. 8, Figs. 9 and 10) computed using the direct results of the non-surrogate method, here considered as the reference, were compared against the impact level predicted by the surrogate method in the four sectors for the three storms. For storm Emma (Fig. 8), the surrogate method overpredicted the impact in one level (low against no impact) in the parking sector during the first integrated time, while the rest of the sectors maintained safe according to the predictions of both approaches. For the second integrated time, additional low impacts were predicted only by the non-surrogate method in the western sector. In the parking sector, the predictions provided by both methods reached high impact. In the remaining sectors, both methods predicted no impact. For the third integrated time, the parking and central sectors were under high impact conditions, the western sector under low impact conditions and the eastern was safe according to the non-surrogate method. The surrogate method displayed similar impacts in the parking and central sectors, and overpredictions for two levels in the western sector and one level in the eastern sector. In the last integrated time, the surrogate method predicted a high impact for all sectors except for the eastern sector (no impact). The non-surrogate method predicted similar impacts in all the sectors except in the western sector. Outside the integrated time, the surrogate method always predicted no impact because the tide level was below 0.5 m (the value of the first bin) while the numerical modeling method predicted no impacts because the EI index did not vary and the scarp toe elevation was invariant.

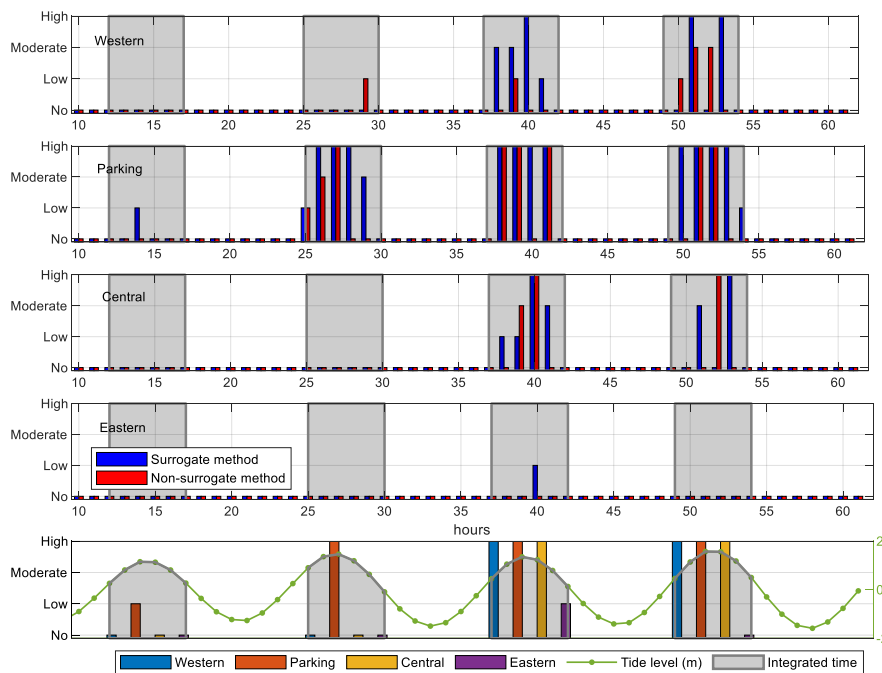Regarding the 6-hour integrated predictions of the synthetic events,

Fig. 8. Storm Emma. Hourly impact level computed directly by the process-based numerical model or non-surrogate method (red bar) and surrogate method (blue bar) in the four sectors. The hours correspond to the beginning of the storm. The bottom plot displays the impact predicted by the surrogate method integrated on the 6 hours centered in the high tide, corresponding to the final alert level of the EWS.
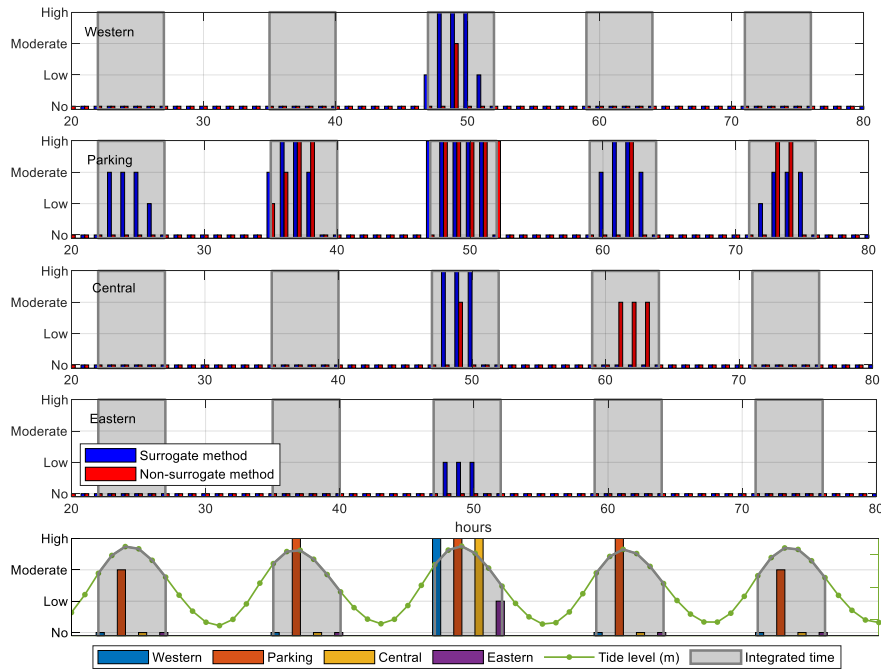
Fig. 9. 10-year event. Hourly impact level computed directly by the process-based numerical model or non-surrogate method (red bar) and surrogate method (blue bar) in the four sectors. The hours correspond to the beginning of the storm. The bottom plot displays the impact predicted by the surrogate method integrated on the 6 hours centered in the high tide, corresponding to the final alert level of the EWS.

Fig. 10. 25-year event. Hourly impact level computed directly by the process-based numerical model or non-surrogate method (red bar) and surrogate method (blue bar) in the four sectors. The hours correspond to the beginning of the storm. The bottom plot displays the impact predicted by the surrogate method integrated on the 6 hours centered in the high tide, corresponding to the final alert level of the EWS.
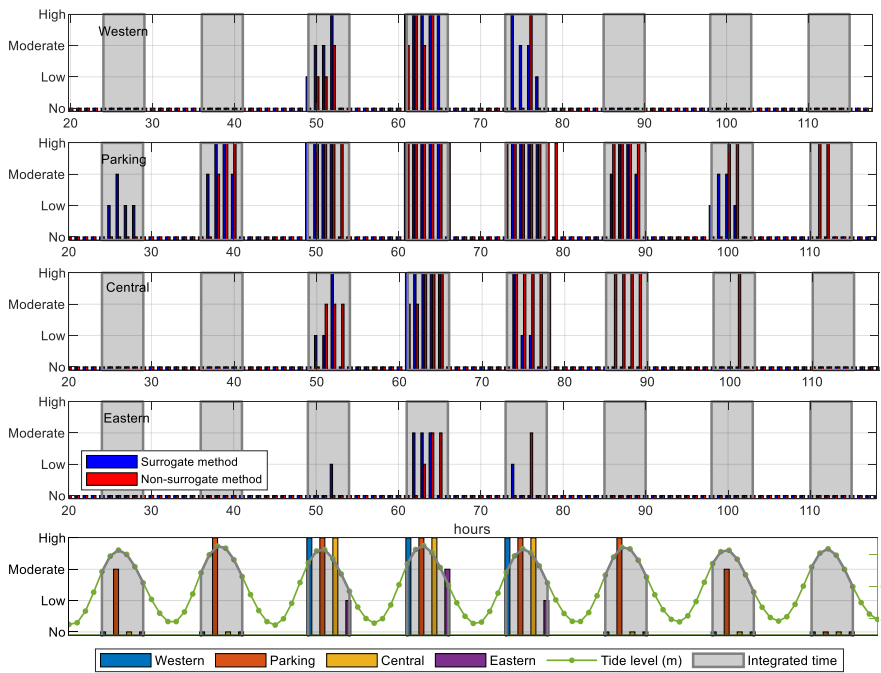
it was found that for the 10-yr event (Fig. 9), the parking sector was the first area to be impacted according to the surrogate method (moderate) in the first integrated time. At the second integrated time, both methods predicted high impact in the parking sector, and no impact in the western, central and eastern sectors. For the third integrated time, at the peak of the storm, the surrogate method anticipated a high impact in

three sectors, namely western, parking and central, and low impact in the eastern sector, while the non-surrogate method predicted one level lower in the western, central and eastern sectors and a similar level in the parking sector. The predictions of the surrogate method for the fourth integrated time matched the reference in the western, parking and eastern sectors and underpredicted the reference by two levels in the

central sector. In the last integrated time, both approaches predicted no impact in the western, central and eastern sectors, while the reference was underpredicted by one level in the parking sector (high impact against moderate impact).

For the 25-yr event (Fig. 10), the surrogate method anticipated moderate impact in the parking sector during the first integrated period, while the non-surrogate method predicted no impact. Both methods estimated no impact in the remaining sectors. During the second integrated time, both methods estimated the same impacts in the four sectors (high impact in the parking and no impact in the other sectors). In the third integrated time, both methods predicted the same impact only in the parking sector. The non-surrogate method predicted moderate impact (western and central sectors) and no impact (eastern sector) and the surrogate method overestimated those predictions on one level. In the fourth integrated time, the peak of the storm, both methods estimated moderate impact in the eastern sector and high impact in the others. In the fifth integrated time, the surrogate method matched the reference in the western, parking and central sectors (high impact) and underpredicted the reference by one level. In the sixth integrated time, both methods agreed in their predictions in three sectors (no impact in the western and eastern sectors and high impact in the parking) but their prediction deviated in the central sector: no impact (surrogate method) against high impact (reference). In the seventh integrated time, the surrogate method underpredicted the reference by one level (moderate against high impact) in the parking and by three levels (no impact against high impact) in the central sector. In the last integrated time, the reference predicted high impact and the surrogate method no impact in the parking sector. In the remaining sectors, both predicted no impact.

To further analyze the predictive skills of the surrogate method, the 6-hour integrated predictions provided by this method were compared with the equivalent 6-hour integrated predictions of the non-surrogate method. This analysis accounted for 17 tidal cycles (4 + 5+8). In general, the ability of the surrogate method to agree with the non-surrogate method for these three events was very positive (Fig. 11) as the accuracy (defined as the match cases divided by all cases) of the 6-hour integrated surrogate method predictions ranged between 64% (parking) and 76% (eastern). Also, the parking and central sectors obtained more cases of underprediction 18%, while in the remaining sectors, the underprediction cases were only 6%. If all sectors and storms were combined, 71% of the cases would match the reference, 19% of the cases would be subject to one level of underprediction or overprediction and 10% of the cases would experience more than 1 level of overprediction or underprediction. Regarding the high impact level, the recall (defined as the relative number of observations that were correctly predicted) varied among sectors with values of 100%, 78% and 67%, in the western, parking and central sectors respectively (high impact level was not predicted either by the surrogate and non-surrogate method in the eastern sector). The precision that expresses the relative number of correct predictions ranged from 40% in the western, 100% in the parking and 67% in the central sector for the high impact level. A more detailed analysis with more statistical skills separating by sectors and levels of impact is shown in the Supplementary material as long with confusion matrixes for the hourly comparison.

3.5.2. Peak of the storm

In this second approach, the widely used *k*-fold cross-validation (Fienen and Plant, 2015) method was followed to assess the predictive and descriptive skills of the model. According to Beuzen et al. (2018), predictive skill indicates the ability of the model to correctly predict events that it has not been trained on, and descriptive skill means the ability of the model to correctly 're-predict' events that it has already been trained on. In the present study, for the computation of the predictive model skills, the BNs were trained with nine folds and their results were tested with the remaining fold (unseen data), while for the descriptive analysis, the BNs were trained with ten folds and tested with one fold (seen data). This exercise was repeated ten times. Finally, the skills (correct answer/total answer) for each individual fold, were averaged to obtain the final model skill. In order to determine the appropriate number of input nodes for BC, three BN configurations were evaluated: two input nodes (Hs, tide level); three input nodes (Hs, tide level, Tp) and four input nodes (Hs, tide level, Tp and Duration, where Duration was discretized in four bins) and the corresponding overfitting ratio (number of runs/number of BN bins, child and parents, required to be learned) was computed.

According to the 10 iterations of the 10-fold cross-validation performed, descriptive model skills were better than the predictive model skills (for more than two input nodes) and the skills increased with the number of nodes (lower overfitting ratio) as displayed in Fig. 12, regardless of the sector. Conversely, the predictive skills did not necessarily improve when increasing the number of nodes. Thus, including the duration node contributed to increase descriptive model skill but the predictive model skills were worse than when comparing to the three node configuration. Beuzen et al. (2018) explained this fact due to a reflection of the model overfitting. They found that with values lower than 1, their BN models become increasingly overfit and that the predictive skill was maximized at an overfitting ratio of approximately 3. In the current work, the predictive skill was maximized at an overfitting ratio of approximately 1 (Fig. 12). Furthermore, the predictive model skills varied between 60% and 70% for the four sectors for the three input node configuration (Fig. 12). This was similar to the accuracy obtained by previous works. For instance, Beuzen et al. (2018) found a maximum prediction skill of 65% and they noticed that their predictive skills were comparable to others reported in other BN coastal studies (Hapke and Plant, 2010; Palmsten et al., 2014) which varied the number of input nodes and training data sizes.

4. Operational phase

After the completion of the development phase and its verification, the operational phase can be initiated. This operational phase does not
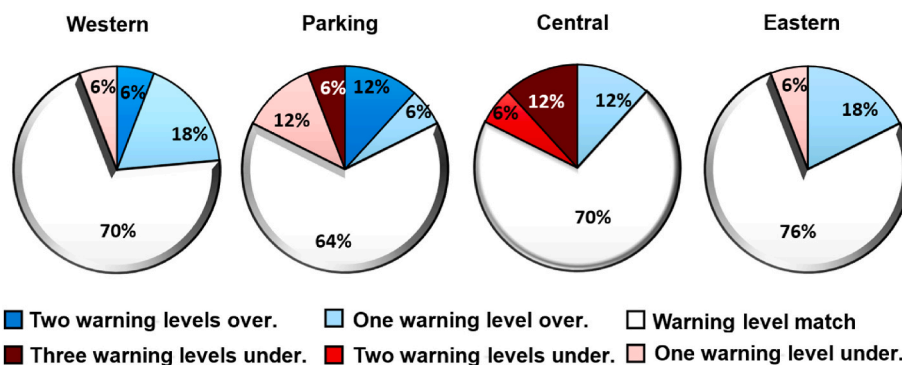

Fig. 11. Overall performance assessment of the surrogate method in the four sectors taking into account a set of 17 predictions.
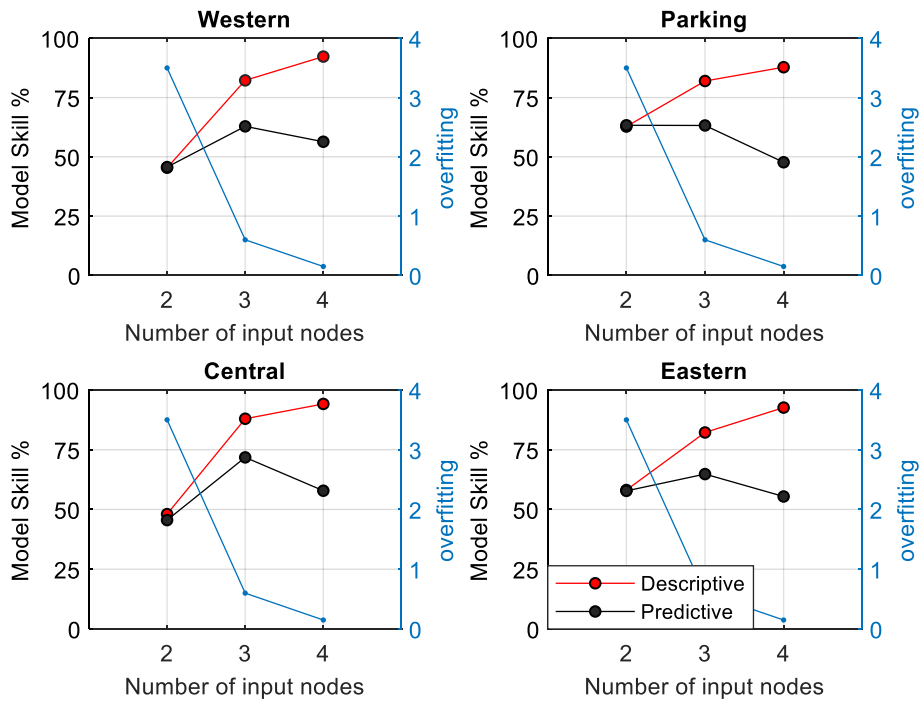
Fig. 12. Analysis of the BN predictive and descriptive skills as a function of the number of boundary conditions nodes and sectors.

require any human intervention and it is an example of an autonomous ML-based EWS. It consists of four main steps: downloading and extracting the oceanic forecasts, introducing these variables into the previously trained BN, obtaining the impact predictions and disseminating the early alerts via email among the final end-users (Fig. 1). The completion of these four steps requires only a few minutes. A set of python scripts were developed to automatize the entire process and implement the EWS within the HIDRALERTA architecture. The hourly impact predictions are produced following the same approach presented in the validation section for the surrogate method and are anticipated for the following 72 hours. Then, they are integrated for a period of 6 hours and released once every day with the latest oceanic forecast information.

The impact predictions at Praia de Faro depend on two types of input conditions. Firstly, estimations of hourly tide levels provided by XTide (www.flaterco.com/xtide) are extracted at the position "Faro – Olhao" for the next 72 hours every day. Secondly, wave parameters, such as spectral significant wave height, wave spectrum peak period and wave direction, forecasted by Puertos del Estado – IBI system (http://opend ap.puertos.es/thredds/fileServer/wave_regional_ibi/HOURLY/) are downloaded. This information can also be obtained via Atlantic-Iberian Biscay Irish- Ocean Physics Analysis and Forecast from the Copernicus Marine Service. The model data has a grid format with a resolution of 0.0833° and the forecast information of the four nodes surrounding the location of the Faro buoy is extracted. Then, these four values are average, and this information is introduced into the BN to predict the impacts at each sector of Praia de Faro.

Usually, BNs work with a graphical interface that allows the user to define the input conditions and infer the results in the same interface. However, for automatized operational purposes, the CPT of the BN generated during the development phase must be autonomously read and the probabilities of each impact level associated with a specific sector and the corresponding BC (wave height, peak period, tide level) must be extracted. The wave direction is used to separate between W-SW ($\geq 180°$) and E-SE events ($<180°$). Storms coming from E-SE are neglected because they cannot create hazardous conditions due to the extreme refraction and the relatively short period, and therefore, their associated impact level is no impact. After the extraction of the probabilities, the criteria and conditions explained in Section 3.5 were applied

in order to deterministically consider the alerts. Furthermore, the impact predictions were integrated for an interval of 6 hours centered on the peak of the tide level. After that, the impact alerts at each sector for the next 72 hours are converted to a color code (Table 1) for a simplified visualization. Finally, this information is printed in a bulletin (see Fig. 13) and disseminated to authorities responsible for the implementation of risk reduction measures.

The alerts generated by HIDRALERTA for Praia de Faro are only disseminated among the authorities and they are not available to the general public. Thus, several end-users or entities with authority to implement or coordinate risk-reduction measures namely the Civil Protection of Faro council, the national and regional divisions of the Portuguese environmental agency (APA) and the Port of Faro are currently receiving this information via email daily. Such information can, however, be made totally or partially available (a larger number of entities), depending on the authorities' policy for each coastal area. In that case, a graphical user interface must be built which the users must access for proper dissemination of the alerts.
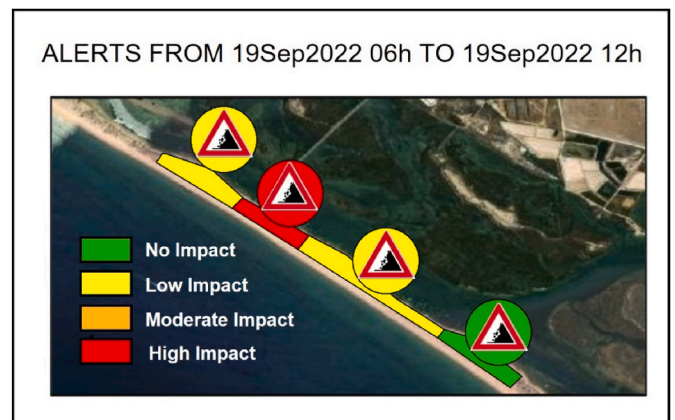

Fig. 13. Illustration of an alert created by the coastal component of HIDRA-LERTA for Praia de Faro (erosion) for the same conditions represented in Fig. 7 and the four sectors. The date and time are merely illustrative.

5. Discussion

5.1. AI for EWS for coastal hazards

Identifying coming natural disasters and releasing early warnings are very cost-effective solutions for disaster preparation (Sättele et al., 2016). ML techniques can serve as a suitable manner to anticipate the coming risks and build efficient forecast systems for natural hazards including extratropical storms (Krishnamurti et al., 2016), precipitation (Shi et al., 2015), earthquakes (Asim et al., 2017), rainfall (Kim et al., 2022), flash-floods (Mane and Mokashi, 2015), coastal flooding (Chondros et al., 2021), tsunamis (Lamsal and Vijay Kumar, 2020), and landslides (Terranova et al., 2015), etc. For coastal hazards, in particular, the development of EWSs supported by machine learning has mainly focused on inundation caused by tsunamis and coastal storm flooding. For tsunamis, several studies have applied machine learning for forecasting and early warning prediction of this hazard and the associated impacts in coastal communities (Fauzi and Mizutani, 2020; Liu et al., 2021; Makinoshima et al., 2021; Mulia et al., 2022). For coastal flooding, there are also several examples of ML-based prediction systems (Callens et al., 2022; Chondros et al., 2021; Denamiel et al., 2019; Dongeren et al., 2018; Fortes et al., 2014; Garzon et al., 2023a; Idier et al., 2021; Pearson et al., 2017). For coastal erosion, while some EWSs have been constructed and implemented (Barnard et al., 2014; Harley et al., 2016; Seok and Suh, 2018; Valchev et al., 2014), they don't consider the utilization of any ML technique. However, some authors (Plomaritis et al., 2018; Poelhekke et al., 2016; Santos et al., 2019) have demonstrated the suitability of BN to support coastal erosion EWSs. Thus, the present study was inspired by these previous studies to create a novel EWS for coastal erosion in sandy beaches and corroborated their outcomes.

5.2. Capabilities for EWS and potential upgrades

The methods exploited in the development phase were based on the work presented by Poelhekke et al. (2016) and utilized their findings for the development of an EWS, although important improvements have been included. (1) The XBeach model built by Poelhekke et al. (2016) only considered up to 20 m depth, but for the development of an EWS, it would be preferable to downscale the hydraulic conditions from deeper waters. Regional operational forecasts that can be used to condition the BN usually face more problems providing reliable predictions near the coast than offshore. In the present study, it has been improved by incorporating a SWAN model coupled with XBeach to generate the training information. This allows the conversion of the hydraulic conditions at 100 m depth in erosion impacts at the coast. (2) The accuracy of the EWS predictions fully depends on the accuracy of the XBeach simulations. The XBeach model used in the present study was developed by Garzon et al. (2022b) and included a detailed calibration, the addition of new model features and model parameters (non-erodible layer and the upslope transport term for semireflective beaches so-called bermslope), an updated topo-bathymetry from 2018 with new elements of the urbanized area and lateral model expansion to cover the entire urbanized area. Garzon et al. (2022b) validated this model against post-storm topographical measurements at five locations for a 16-year return period event and four locations for a 5-year return period event with a qualification of excellent according to the van Rijn et al. (2003) classification. This upgrading of the numerical model represents a large improvement with respect to previous models developed in Praia de Faro in Poelhekke et al. (2016). (3) Another novel aspect of this study was the development of hourly and time-integrated predictions since previous studies have not dealt with the timing and evolution of the storm impacts. (4) The definition of the EI index (as a proxy for coastal erosion) and the characterization of the impacts through its limits shown in Table 1 were novel since a quantitative and qualitative definition of the impacts is not often provided in this type of studies. (5) In the present

study, the number of synthetic events for training the BN was higher than in previous studies developed at Praia de Faro, with a reduction of the bin size of the Hs and Tp variables for a better characterization of the oceanic conditions and thus lower spread of the probability distributions of the impact predictions.

Making accurate predictions with AI techniques typically requires a large amount of good data. The developed prediction system presented in this study combines ML techniques with morphodynamic models to implement a reliable and efficient EWS for coastal erosion in sandy beaches. Since storm impact observations that cover a long period are not available at the study site (nor at most sites worldwide), process-based modeling was used instead to generate this information. Therefore, this approach accounted for the dominant physical mechanisms that govern wave propagation and transformation and morphological evolution to make predictions of storm impacts on sandy beaches, as an alternative to other more computationally efficient, but less accurate methods such as the Convolution or the ShoreFor model (Plomaritis et al., 2019a).

The inclusion of all generated data into the AI technique to automatically and quasi-immediately provide storm impacts was a key aspect to guarantee the release of alerts in a short period of time between the successively updated wave forecasts. Whether a non-surrogate method would have been implemented, simulating 72 hours of erosion by running SWAN + XBeach would take more than 6 hours on four logical processors in a 1600x Six-Core Processor, 3600 Mhz workstation. Wave operational models that can be employed as BC offer a 3–5 day forecast window (at least with a certain degree of reliability) and they are updated every 12 or 24 hours. Thus, coastal erosion model simplifications to increase the EWS operability should have been considered since most probably the results of a complex modeling approach would not be available at the time of issuing the alerts that account for the updated BC. Moreover, the construction of the EWS in two separate phases also contributes to simplifying the maintenance of the system and limiting the computational power required to operate the system since most of the modeling efforts are undertaken beforehand. This methodology developed here was implemented in Praia de Faro, but it can be transferred to other sandy beaches with some adaptations to the local characteristics such as the definition of the synthetic storms, the choice of the regional forecast system to condition the impact predictions or the selection of the most appropriate beach morphology.

Importantly, the EWS structure enables the development and operational phases can be built on different machines increasing the flexibility for its implementation. Another advantage of the developed BN-based EWS is that new modules and information can be generated independently and added to the existing system. For instance, if new nodes and bins are necessary, then the BN can be extended. All runs could be performed outside the system, train the BN, and afterward implement and update the EWS. This includes the possibility of integrating different beach morphologies, and wave and sea level conditions in a flexible way. As the reliability of the BC prediction might increase in the future (namely for wave forecast) the output of the EWS can be also extended in time, from the current 72 hours to a longer limit without compromising the execution time of the operational phase.

The complexity of the used surrogate method can also be increased. Social behaviors can be tested and incorporated as nodes of the BN, being, therefore, this aspect considered on the risk level assessment. Moreover, different levels of potential occupation can be included, for instance integrating the expected beach occupation as a function of the hour (e.g. morning, afternoon, night) or the weekday (e.g. weekend versus working day). Therefore, all this can be incorporated into the already developed ML scheme and still quasi-immediately provide results, after the implementation of such adjustments on the BN-based EWS.

5.3. Uncertainties and limitations

Relevant variables of a storm for driving coastal erosion such as duration and surge were not explicitly included in the BN, but the copula methodology exploited here to generate the synthetic storms attempted to characterize their natural variability. This largely reduced the number of runs to be simulated and thus it had a significant impact on the time devoted to modeling coastal erosion on the numerical framework and generating the training information. The downside of this approach was that some uncertainty was added to the predictions, especially for extreme events where storm duration can regulate the capacity of the dune to withstand or be dismantled (Garzon et al., 2023b). However, this uncertainty was reduced by considering up to four storms per Hs-Tp bin to train the BN, since the more runs were added, the better the natural variability was captured. Another important aspect was that the temporal variation of the bulk parameters of the storms was assumed to follow a symmetric triangular evolution. It was made based on the numerical experiments performed by Garzon et al. (2023b) that found this approach can appropriately replicate the erosion caused by large storms in Praia de Faro. On the other hand, other authors (Duo et al., 2020) have questioned the validity of the symmetric triangular approach to imitate the impact of real storms stating that it increases the error of the prediction when compared to the modeling of the actual shape of the storm. However, for the development of this type of EWS where the storms are previously modeled, it is impossible to know in advance the storm shape, and assumptions like the triangular shape (or other) must be made.

The EWS does not consider an updated topography when initializing the model simulations. This can arise another source of uncertainty in the EWS predictions since variations between the actual pre-storm topography and the one considered in the XBeach simulations can be found. Previous studies (Beuzen et al., 2019; Garzon et al., 2022a; Garzon et al., 2023b) have highlighted that beach width and sediment volume of the aerial beach can control the post-storm profile, and thus, these variations can lead to differences in the response of the beach dune systems. Here, the profile implemented in the numerical model corresponded to a set of measurements carried out in late 2018. The field campaign was conducted several months after the impact of the storm Emma when the profile had already recovered almost its entire volume. Therefore, the pre-storm topography implemented in the numerical model corresponded to a beach morphology under non-erosive conditions. Malvarez et al. (2021) declared that Praia de Faro has a good ability to recover from the impact of large storms (more than 70% recovery in one month) and it would indicate that the uncertainty associated with the pre-storm morphology would be lower in comparison with other sites with longer periods to recover its pre-storm morphology. Nevertheless, in case the site is impacted previously by an energetic storm without sufficient time to recover before the impact of a second storm, it can propagate uncertainties in the simulated dune retreat of around 14%–41% and up to 88% of the berm retreat, depending on the storm severity (Garzon et al., 2023b). The best solution would be to test, model and implement the storm impacts for several different beach profiles at the BN, and then select the beach profile most similar to the existing one at each time (this would also require continuous beach monitoring in the considered sectors).

Obtaining continuous topographical measurements of the beach profile during a storm is a very challenging task, and therefore the authors used instead a calibrated and validated numerical model framework (non-surrogate method) to assess the predictive accuracy of the Surrogate method. As displayed in Fig. 11, the Surrogate method predictions achieved a good level of agreement when compared to the non-surrogate method for the four sectors evaluated within the integrated time. Moreover, for the implementation in an EWS, the surrogate method would be also appropriate since it can identify the specific hours when there was a direct action with potential consequences and when the hazardous conditions disappeared. The purpose of conventional warning systems would be to alert only when the risk will occur, but these prediction systems do not release an alert due to risks that can remain on the site for hours or even days as a consequence of hazardous past conditions.

The variation of the impact level predicted by the surrogate method within a tide cycle was not very significant but the unification of these predictions in just one level for 6 hours can largely simplify the implementation of the risk reduction measures by the authorities. The EI index used to classify those impact levels has been implemented for the first time in a risk analysis assessment. Thus, the thresholds considered to separate between levels of impact were established based on the authors' judgment and expertise for the study area. More comprehensive analyses that involve field observations might be required to evaluate the ability of this index to anticipate storm impacts in this and additional sites. From the numerical perspective, increasing the resolution of the erosion model might contribute to a more precise estimation of D and h, but cross-shore resolutions of 1–2 m are considered appropriate for this type of application.

6. Conclusions

The design, building, and implementation of a novel BN-based Early Warning System for coastal erosion in sandy beaches are presented. This system combines machine learning techniques, namely Bayesian Networks, and state-of-the-art numerical models, such as XBeach and SWAN, to predict storm erosion impacts in urbanized areas. This system was developed in two phases: development and operational. In the development phase, all information required to apply the machine learning method was generated, including the definition of hundreds of oceanic synthetic storms, modeling of the erosion caused by these storms, and characterization of the impact levels according to a newly defined erosion impact index. This adimensional index relates the horizontal distance from the edge of the dune/beach scarp to buildings and the height of that scarp. Finally, a Bayesian Network that acted as a surrogate of the previously generated information was built. After the training of the network, conditional probability tables were created. These tables constituted the ground knowledge to make the predictions in the second phase. The development phase represented a further step in the work presented by Poelhekke et al. (2016), which was a proof of concept for the same study area, with an emphasis on operational systems.

The methodology designed during the implementation phase was validated following two approaches. Firstly, by comparing results from the BN (surrogate method) against data obtained from running the models (non-surrogate method), here considered as the reference. This comparison considered the entire duration of three large storms whose return periods were 10, 16 and 25 years and it was observed that the surrogate method correctly predicted between 65% and 75% of the impacts. The remaining cases were mainly either overpredicted or underpredicted by one level, especially for the western and eastern sectors. Furthermore, the surrogate method was able to separate when a direct action with potential consequences was happening and when the hazardous conditions disappeared. Secondly by using the iterative *k*-fold cross-validation procedure where the BN was trained with nine folds and tested with one fold (only for the peak of the storm). This unbiased procedure was applied for three different BN configurations and it revealed that three input nodes for the oceanic BCs maximized the predictive BN skills (63%–72%).

Simulating beach erosion for 72 hours by running SWAN + XBeach operationally would take more than 6 hours on a four-logical processor workstation (against the few minutes required to complete the operational phase) with a slightly better level of predictive skills than the surrogate method, as found on the hourly comparison assessment. Hence, this study demonstrated that the two-phase approach developed here can fastly provide high-accuracy predictions of erosion impacts. Praia de Faro was selected as the demonstration site but the

methodology designed here can be easily applied to other areas worldwide with some modifications (e.g., the creation of synthetic storms) or adapted to incorporate other numerical models instead of SWAN and XBeach. Moreover, the modular architecture with two working phases is very flexible enabling the inclusion of additional features such as beach morphology characteristics, human occupation, social behavior, new oceanic conditions and longer prediction periods constituting a powerful tool for disaster management.

CRediT authorship contribution statement

J.L. Garzon: Writing – review & editing, Writing – original draft, Validation, Methodology, Investigation, Formal analysis, Conceptualization. **O. Ferreira:** Writing – review & editing, Supervision, Project administration, Methodology, Funding acquisition, Conceptualization. **T.A. Plomaritis:** Writing – review & editing, Supervision, Methodology, Conceptualization. **A.C. Zózimo:** Writing – review & editing, Software, Methodology. **C.J.E.M. Fortes:** Writing – review & editing, Software, Project administration, Methodology. **L.V. Pinheiro:** Visualization, Software.

Declaration of competing interest

The authors declare that they have no known competing financial interests or personal relationships that could have appeared to influence the work reported in this paper.

Data availability

Data will be made available on request.

Acknowledgments

Appendix A. Supplementary data

Supplementary data to this article can be found online at https://doi.org/10.1016/j.coastaleng.2024.104460.

References

Aguilera, P.A., Fernández, A., Fernández, R., Rumí, R., Salmerón, A., 2011. Bayesian networks in environmental modelling. Environ. Model. Software 26, 1376–1388. https://doi.org/10.1016/j.envsoft.2011.06.004.

Almeida, L.P., 2007. Variabilidade do Perfil de Praia em Função da Agitação Marítima. In: Proj. Técnico-científico da Licenciatura em Oceanogr. Univ. do Algarve, Fac. Ciências e do Ambient, Faro.

Almeida, L.P., Vousdoukas, M.V., Ferreira, Ó., Rodrigues, B.A., Matias, A., 2012. Thresholds for storm impacts on an exposed sandy coastal area in southern Portugal. Geomorphology 143–144, 3–12. https://doi.org/10.1016/j.geomorph.2011.04.047.

Asim, K.M., Martínez-Álvarez, F., Basit, A., Iqbal, T., 2017. Earthquake magnitude prediction in Hindukush region using machine learning techniques. Nat. Hazards 85, 471–486. https://doi.org/10.1007/s11069-016-2579-3.

Athanasiou, P., Dongeren, A., Van Giardino, A., Vousdoukas, M., Jose, A.A., Ranasinghe, R., 2022. Estimating dune erosion at the regional scale using a meta-model based on neural networks. Nat. Hazards Earth Syst. Sci. 1–30. https://doi.org/10.5194/nhess-2022-106.

Banan-Dallalian, M., Shokatian-Beiragh, M., Golshani, A., Abdi, A., 2023. Use of a Bayesian network for storm-induced flood risk assessment and effectiveness of ecosystem-based risk reduction measures in coastal areas (Port of Sur, Sultanate of Oman). Ocean Eng. 270, 113662. https://doi.org/10.1016/j.oceaneng.2023.113662.

Barnard, P.L., van Ormondt, M., Erikson, L.H., Eshleman, J., Hapke, C., Ruggiero, P., Adams, P.N., Foxgrover, A.C., 2014. Development of the Coastal Storm Modeling System (CoSMoS) for predicting the impact of storms on high-energy, active-margin coasts. Nat. Hazards 74, 1095–1125. https://doi.org/10.1007/s11069-014-1236-y.

Beuzen, T., Harley, M.D., Splinter, K.D., Turner, I.L., 2019. Controls of variability in berm and dune storm erosion. J. Geophys. Res. Earth Surf 124, 2647–2665. https://doi.org/10.1029/2019JF005184.

Beuzen, T., Splinter, K.D., Marshall, L.A., Turner, I.L., Harley, M.D., Palmsten, M.L., 2018. Bayesian Networks in coastal engineering: distinguishing descriptive and predictive applications. Coast Eng. 135, 16–30. https://doi.org/10.1016/j.coastaleng.2018.01.005.

Brodie, K.L., Spore, N., 2015. Foredune classification and storm response: automated analysis of terrestrial Lidar Dems. Coastal sediments 2015. https://doi.org/10.1142/9789814689977_0041.

Bruno, D.E., Barca, E., Goncalves, R.M., de Araujo Queiroz, H.A., Berardi, L., Passarella, G., 2018. Linear and evolutionary polynomial regression models to forecast coastal dynamics: comparison and reliability assessment. Geomorphology 300, 128–140. https://doi.org/10.1016/j.geomorph.2017.10.012.

Callens, A., Morichon, D., Liquet, B., 2022. Bayesian networks to predict storm impact using data from both monitoring networks and statistical learning methods. Nat. Hazards 115, 2031–2050. https://doi.org/10.1007/s11069-022-05625-z.

Charbonneau, B.R., Wootton, L.S., Wnek, J.P., Langley, J.A., Posner, M.A., 2017. A species effect on storm erosion: invasive sedge stabilized dunes more than native grass during Hurricane Sandy. J. Appl. Ecol. 54, 1385–1394. https://doi.org/10.1111/1365-2664.12846.

Chondros, M., Tsoukala, V., Metallinos, A., Papadimitriou, A., Memos, C., 2021. A coastal flood early-warning system based on offshore sea state forecasts and artificial neural networks. J. Mar. Sci. Eng. 9 https://doi.org/10.3390/jmse9111272.

Ciavola, P., Taborda, R., Ferreira, Ó., Dias, J.A., 1997. Field observations of sand-mixing depths on steep beaches. Mar. Geol. 141, 147–156. https://doi.org/10.1016/S0025-3227(97)00054-6.

Denamiel, C., Šepić, J., Huan, X., Bolzer, C., Vilibić, I., 2019. Stochastic surrogate model for meteotsunami early warning system in the eastern adriatic sea. J. Geophys. Res. Ocean 124, 8485–8499. https://doi.org/10.1029/2019JC015574.

Dongeren, A.Van, Ciavola, P., Martinez, G., Viavattene, C., Bogaard, T., Ferreira, O., Higgins, R., Mccall, R., 2018. Introduction to RISC-KIT: resilience-increasing strategies for coasts. Coast Eng. 134, 2–9. https://doi.org/10.1016/j.coastaleng.2017.10.007.

Duo, E., Sanuy, M., Jiménez, J.A., Ciavola, P., 2020. How good are symmetric triangular synthetic storms to represent real events for coastal hazard modelling. Coast Eng. 159 https://doi.org/10.1016/j.coastaleng.2020.103728.

Fauzi, A., Mizutani, N., 2020. Machine learning algorithms for real-time tsunami inundation forecasting: a case study in Nankai region. Pure Appl. Geophys. 177, 1437–1450. https://doi.org/10.1007/s00024-019-02364-4.

Ferreira, Ó., Martins, J.T., Dias, J.A., 1997. Morfodinâmica e vulnerabilidade da Praia de Faro. In: Livro Comun. do Semin. Sobre a Zo. Costeira do Algarve, EUROCOAST Port, pp. 67–76.

Ferreira, Ó., Plomaritis, T.A., Costas, S., 2019. Effectiveness assessment of risk reduction measures at coastal areas using a decision support system: findings from Emma storm. Sci. Total Environ. 657, 124–135. https://doi.org/10.1016/j.scitotenv.2018.11.478.

Ferreira, Ó., Taborda, R., Dias, J.A., 1998. Morphological vulnerability index: a simple way of determining beach behaviour. Coast Eng. 3206–3214. https://doi.org/10.1061/9780784404119.243.

Fienen, M.N., Plant, N.G., 2015. A cross-validation package driving Netica with python. Environ. Model. Software 63, 14–23. https://doi.org/10.1016/j.envsoft.2014.09.007.

Fortes, C.J.E.M., Reis, M.T., Pinheiro, L., Poseiro, P., Serrazina, V., Mendonça, A., Smithers, N., Santos, M.I., Barateiro, J., Azevedo, E.B., Salvador, M., Reis, F.V., 2020. The HIDRALERTA system: application to the ports of Madalena do Pico and S. Roque do Pico, Azores. Aquat. Ecosyst. Health Manag. 23, 398–406. https://doi.org/10.1080/14634988.2020.1807295.

Fortes, C.J.E.M., Reis, M.T., Poseiro, P., Santos, J.A., Pinheiro, L., Craveiro, J., Rodrigues, A., Sabino, A., Silva, S.F., Ferreira, J.C., Raposeiro, P., Silva, C., Rodrigues, M.C., Simões, A., Azevedo, E.B., Reis, F., 2014. HIDRALERTA project: a flood forecast and alert system in coastal and port areas. In: IWA World Water Congress and Exhibition. https://doi.org/10.13140/2.1.3697.1524.

Garzon, J.L., Costas, S., Ferreira, Ó., 2022a. Biotic and abiotic factors governing dune response to storm events. Earth Surf Process Landforms 47, 1013–1031. https://doi.org/10.1002/esp.5300.

Garzon, J.L., Ferreira, O., Plomaritis, T.A., 2022b. Modeling of coastal erosion in exposed and groin-protected steep. J. Waterw. Port, Coast. Ocean Eng. 148, 1–26. https://doi.org/10.1061/(ASCE)WW.1943-5460.0000719.

Garzon, J.L., Ferreira Zózimo, A.C., Fortes, C.J.E.M., Ferreira, A.M., Pinheiro, L.V., Reis, M.T., 2023a. Development of a Bayesian networks-based early warning system for wave-induced flooding. Int. J. Disaster Risk Reduc. 96, 1–19. https://doi.org/10.1016/j.ijdrr.2023.103931.

Garzon, J.L., Plomaritis, T.A., Ferreira, O., 2023b. Uncertainty analysis related to beach morphology and storm duration for more reliable early warning systems for coastal hazards. J. Geophys. Res. Ocean 1–21. https://doi.org/10.1029/2022JC019339.

Goldstein, E.B., Coco, G., Plant, N.G., 2019. A review of machine learning applications to coastal sediment transport and morphodynamics. Earth Sci. Rev. 194, 97–108. https://doi.org/10.1016/j.earscirev.2019.04.022.

Goldstein, E.B., Moore, L.J., 2016. Stability and bistability in a one-dimensional model of coastal foredune height. J. Geophys. Res. Surf 964–977.

Grimes, D.J., Cortale, N., Baker, K., McNamara, D.E., 2015. Nonlinear forecasting of intertidal shoreface evolution. Chaos 25. https://doi.org/10.1063/1.4931801.

Gutierrez, B.T., Plant, N.G., Thieler, E.R., 2011. A Bayesian network to predict coastal vulnerability to sea level rise. J. Geophys. Res. Earth Surf 116, 1–15. https://doi.org/10.1029/2010JF001891.

Haerens, P., 2009. Seasonal and storm induced morphological variations at Praia de Faro, Península do Ancão, Southern Portugal.

Hapke, C., Plant, N., 2010. Predicting coastal cliff erosion using a Bayesian probabilistic model. Mar. Geol. 278, 140–149. https://doi.org/10.1016/j.margeo.2010.10.001.

Harley, M.D., Valentini, A., Armaroli, C., Perini, L., Calabrese, L., Ciavola, P., 2016. Can an early-warning system help minimize the impacts of coastal storms? A case study of the 2012 Halloween storm, northern Italy. Nat. Hazards Earth Syst. Sci. 16, 209–222. https://doi.org/10.5194/nhess-16-209-2016.

Idier, D., Aurouet, A., Bachoc, F., Baills, A., Betancourt, J., Gamboa, F., Klein, T., López-Lopera, A.F., Pedreros, R., Rohmer, J., Thibault, A., 2021. A user-oriented local coastal flooding early warning system using metamodelling techniques. J. Mar. Sci. Eng. 9 https://doi.org/10.3390/jmse9111191.

IPCC, 2012. Managing the Risks of Extreme Events and Disasters to Advance Climate Change Adaptation. In: Field, C.B., Barros, V., Stocker, T.F., Qin, D., Dokken, D.J., Ebi, K.L., Mastrandrea, M.D., Mach, K.J., Plattner, G.-K., Allen, S.K., Tignor, M., Midgley, P.M. (Eds.), 2012.A Special Report of Working Groups I and II of the Intergovernmental Panel on Climate Change. Cambridge. ed., Cambridge, UK/New York. https://doi.org/10.1017/CBO9781139177245.009.

Jäger, W.S., Christie, E.K., Hanea, A.M., den Heijer, C., Spencer, T., 2018. A Bayesian network approach for coastal risk analysis and decision making. Coast Eng 134, 48–61. https://doi.org/10.1016/j.coastaleng.2017.05.004.

Kim, T., Yang, T., Zhang, L., Hong, Y., 2022. Near real-time hurricane rainfall forecasting using convolutional neural network models with Integrated Multi-satellitE Retrievals for GPM (IMERG) product. Atmos. Res. 270, 106037. https://doi.org/10.1016/j.atmosres.2022.106037.

Krishnamurti, T.N., Kumar, V., Simon, A., Bhardwaj, A., Ghosh, T., Ross, R., 2016. A review of multimodel superensemble forecasting for weather, seasonal climate, and hurricanes. Rev. Geophys. 54, 336–377. https://doi.org/10.1002/2015RG000513.

Kuglitsch, M., Albayrak, A., Aquino, R., Craddock, A., Edward-Gill, J., Kanwar, R., Koul, A., Ma, J., Marti, A., Menon, M., Pelivan, I., Toreti, A., Venguswamy, R., Ward, T., Xoplaki, E., Rea, A., Luterbacher, J., 2022. Artificial intelligence for disaster risk reduction: opportunities. Chall. Prospects 1–14.

Lamsal, R., Vijay Kumar, T.V., 2020. Artificial Intelligence Based Early Warning System for Coastal Disasters, pp. 305–320. https://doi.org/10.1017/978-981-15-4294-7_21.

Liu, C.M., Rim, D., Baraldi, R., LeVeque, R.J., 2021. Comparison of machine learning approaches for tsunami forecasting from sparse observations. Pure Appl. Geophys. 178, 5129–5153. https://doi.org/10.1007/s00024-021-02841-9.

López, I., Aragonés, L., Villacampa, Y., Serra, J.C., 2017. Neural network for determining the characteristic points of the bars. Ocean Eng. 136, 141–151. https://doi.org/10.1016/j.oceaneng.2017.03.033.

Makinoshima, F., Oishi, Y., Yamazaki, T., Furumura, T., Imamura, F., 2021. Early forecasting of tsunami inundation from tsunami and geodetic observation data with convolutional neural networks. Nat. Commun. 12, 1–10. https://doi.org/10.1038/s41467-021-22348-0.

Malvarez, G., Ferreira, O., Navas, F., Cooper, J.A.G., Gracia-Prieto, F.J., Talavera, L., 2021. Storm impacts on a coupled human-natural coastal system : Resilience of developed coasts. Sci. Total Environ. 768, 144987 https://doi.org/10.1016/j.scitotenv.2021.144987.

Mane, S.S., Mokashi, M.K., 2015. Real-time flash-flood monitoring, alerting and forecasting system using data mining and wireless sensor network. In: 2015 Int. Conf. Commun. Signal process. ICCSP 2015, pp. 1881–1886. https://doi.org/10.1109/ICCSP.2015.7322851.

Masselink, G., Short, A.D., 1993. The effect of tide range on beach morphodynamics and morphology: a conceptual beach model. J. Coast Res.. 9 (3), 785–800.

Mendes, D., Oliveira, T.C.A., 2021. Deep-water spectral wave steepness offshore mainland Portugal. Ocean Eng. 236, 109548 https://doi.org/10.1016/j.oceaneng.2021.109548.

Mihaljević, B., Bielza, C., Larrañaga, P., 2021. Bayesian networks for interpretable machine learning and optimization. Neurocomputing 456, 648–665. https://doi.org/10.1016/j.neucom.2021.01.138.

Mulia, I.E., Ueda, N., Miyoshi, T., Gusman, A.R., Satake, K., 2022. Machine learning-based tsunami inundation prediction derived from offshore observations. Nat. Commun. 13 https://doi.org/10.1038/s41467-022-33253-5.

NOAA National Centers for Environmental Information (NCEI), 2022. U.S. Billion-Dollar Weather and Climate Disasters (2022) [WWW Document]. URL. https://www.ncei.noaa.gov/access/billions. (Accessed 10 January 2022).

Palmsten, M.L., Splinter, K.D., Plant, N.G., Stockdon, H.F., 2014. Probabilistic estimation of dune retreat on the Gold Coast, Australia. Shore \& Beach 82, 35–43.

Pape, L., Kuriyama, Y., Ruessink, B.G., 2010. Models and scales for cross-shore sandbar migration. J. Geophys. Res. Earth Surf 115, 1–13. https://doi.org/10.1029/2009JF001644.

Pearson, S.G., Storlazzi, C.D., van Dongeren, A.R., Tissier, M.F.S., Reniers, A.J.H.M., 2017. A Bayesian-based system to assess wave-driven flooding hazards on coral Reef-Lined coasts. J. Geophys. Res. Ocean 122, 10099–10117. https://doi.org/10.1002/2017JC013204.

Pires, H.O., 1998. Project INDIA. Preliminary Report on Wave Climate at Faro. Instituto de Meteorologia, IST, Lisboa, Portugal.

Plant, N.G., Stockdon, H.F., 2012. Probabilistic prediction of barrier-island response to hurricanes. J. Geophical Res. 117, 1–17. https://doi.org/10.1029/2011JF002326.

Plomaritis, T.A., Costas, S., Ferreira, O., 2018. Use of a Bayesian network for coastal hazards, impact and disaster risk. Coast. Eng 134, 134–147. https://doi.org/10.1016/j.coastaleng.2017.07.003.

Plomaritis, Theocharis A., Ferreira, Ó., Costas, S., 2019a. VALIDATION of a Bayesian based early warning system for coastal hazards: the EMMA storm impact at faro beach (south Portugal). Coastal Sediments 2019, 1447–1459. https://doi.org/10.1142/9789811204487_0126.

Plomaritis, T.A., Ferreira, Ó., Costas, S., Puig, M., 2019b. Storm induced coastal erosion: indicators selection and comparison of three modelling approaches. X Jornadas de Geomorfología Litoral 37–40.

Poelhekke, L., Jäger, W.S., van Dongeren, A., Plomaritis, T.A., McCall, R., Ferreira, Ó., 2016. Predicting coastal hazards for sandy coasts with a Bayesian network. Coast. Eng 118, 21–34. https://doi.org/10.1016/j.coastaleng.2016.08.011.

Rodrigues, B.A., Matias, A., Ferreira, Ó., 2012. Overwash hazard assessment. Geol. Acta 10, 427–437. https://doi.org/10.1344/105.000001743.

Santos, V.M., Wahl, T., Long, J.W., Passeri, D.L., Plant, N.G., 2019. Combining numerical and statistical models to predict storm-induced dune erosion. J. Geophys. Res. Earth Surf 1817–1834. https://doi.org/10.1029/2019JF005016.

Sanuy, M., Jiménez, J.A., 2021. Probabilistic characterisation of coastal storm-induced risks using Bayesian networks. Nat. Hazards Earth Syst. Sci. 21, 219–238. https://doi.org/10.5194/nhess-21-219-2021.

Sanuy, M., Jiménez, J.A., Plant, N., 2020. A Bayesian network methodology for coastal hazard assessments on a regional scale: the BN-CRAF. Coast. Eng 157, 1–10. https://doi.org/10.1016/j.coastaleng.2019.103627.

Sättele, M., Bründl, M., Straub, D., 2016. Quantifying the effectiveness of early warning systems for natural hazards. Nat. Hazards Earth Syst. Sci. 16, 149–166. https://doi.org/10.5194/nhess-16-149-2016.

Seok, J.S., Suh, S.W., 2018. Efficient real-time erosion early warning system and artificial sand dune Breaching on Haeundae beach, Korea. J. Coast. Res. 85, 186–190. https://doi.org/10.2112/SI85-038.1.

Shi, X., Chen, Z., Wang, H., Yeung, D.Y., Wong, W.K., Woo, W.C., 2015. Convolutional LSTM network: a machine learning approach for precipitation nowcasting. Adv. Neural Inf. Process. Syst 2015-Janua, 802–810.

Smith, A., Houser, C., Lehner, J., George, E., Lunardi, B., 2020. Crowd-sourced identification of the beach-dune interface. Geomorphology 367, 107321. https://doi.org/10.1016/j.geomorph.2020.107321.

Sun, W., Bocchini, P., Davison, B.D., 2020. Applications of artificial intelligence for disaster management, Natural Hazards. Springer, Netherlands. https://doi.org/10.1007/s11069-020-04124-3.

Terranova, O.G., Gariano, S.L., Iaquinta, P., Iovine, G.G.R., 2015. GASAKe: forecasting landslide activations by a genetic-algorithms-based hydrological model. Geosci. Model Dev. 8, 1955–1978. https://doi.org/10.5194/gmd-8-1955-2015.

Valchev, N., Andreeva, N., Eftimova, P., Trifonova, E., 2014. Prototype of early warning system for coastal storm hazard (Bulgarian black sea \coast). Comptes Rendus L'Academie Bulg. des Sci. 67, 971–978.

van Rijn, L.C., Wasltra, D.J.R., Grasmeijer, B., Sutherland, J., Pan, S., Sierra, J.P., 2003. The predictability of cross-shore bed evolution of sandy beaches at the time scale of storms and seasons using process-based profile models. Coast Eng 47, 295–327. https://doi.org/10.1016/S0378-3839(02)00120-5.

van Verseveld, H.C.W., van Dongeren, A.R., Plant, N.G., Jäger, W.S., den Heijer, C., 2015. Modelling multi-hazard hurricane damages on an urbanized coast with a Bayesian network approach. Coast. Eng 103, 1–14. https://doi.org/10.1016/j.coastaleng.2015.05.006.

Vousdoukas, M.I., Almeida, L.P.M., Ferreira, Ó., 2012. Beach erosion and recovery during consecutive storms at a steep-sloping, meso-tidal beach. Earth Surf. Process. Landforms 37, 583–593. https://doi.org/10.1002/esp.2264.